Synthesis of Porous CoO Nanorods @ N-doped Carbon as High-Performance Lithium Ion Battery Anode

Chenhao Zhao[1,2], Ye Shen[1], Zhibiao Hu[1,2,] and Xinxin Wang[3]*

[1] College of Chemistry & Materials Science, LongYan University, Fujian LongYan, 364012, China.
[2] Fujian Provincial Key Laboratory of Clean Energy Materials, LongYan University, Fujian LongYan, 364012, China.
[3] School of Chemical and Biological Engineering, QiLu Institute of Technology, Shandong Jinan, 250200, China.
[*]E-mail: zhibiaohu@163.com

Construction of porous-structure and carbon coated transition metal oxides is essential for their use as lithium ion battery anodes. In this study, CoO nanorods @ N-doped carbon have been prepared via a synchronous carbonization/reduction of Co_3O_4 nanorods @ polypyrrole composite. XRD patterns suggest the pure-phase CoO can be obtained when the added amount of pyrrole reaches an amount of 180 μL. SEM and TEM images show CoO with surface carbon layer can well inherit the porous nanorod structure of Co_3O_4 template, and partial nitrogen is doped into carbon backbone. As lithium ion battery anode, the optimal sample obtained at a pyrrole content of 270 μL can deliver an initial discharge capacity of 923.9 mAh g^{-1} with high Coulombic efficiency of 75.6% at 200 mAg^{-1}, and a capacity value of 841.6 mAh g^{-1} can be kept after 100 cycles. Even at a high rate of 1000 mAg^{-1}, a stable discharge capacity of 570 mAh g^{-1} can also be reached. These promising electrochemical performances may be attributed to the synergistic effect of porous structure and carbon coating.

1. INTRODUCTION

To meet the increasing requirement of lithium ion batteries (LIBs) with high discharge capacity and good cycling stability, high-performance anode materials have been intensively developed compared with commercial carbon-based anodes [1-3]. Among them, the cobalt-based oxides such as Co_3O_4[4-8], CoO [9-16] and $ZnCo_2O_4$ [17-20] also have attracted a great amount of attention due to their high theoretical discharge capacity (600-1000 mAh g^{-1}) accompanying with a high initial

Coulombic efficiency. In fact, the cobalt-based oxides especially spinel-structure cobalt oxides (Co_3O_4 and ACo_2O_4) can reach a practical discharge capacity of over 1000 mAh g^{-1} [21]. For example, the hierarchical self-assemble $MnCo_2O_4$ nanoflakes prepared by Mn-Co binary carbonate nanoflakes can deliver a reversible discharge capacity of 1094 mAh g^{-1} at 50 mA g^{-1} at the initial cycle, and a capacity of 925 mAh g^{-1} can be retained after 50 cycles at 100 mA g^{-1} [21].

However, the poor cycling stability and rate capability of cobalt based oxides resulting from low electric conductivity and mechanical stress limit their practical application. In order to overcome these problems and improve their electrochemical performances, one of effective strategies is to design the nanostructured porous or hollow electrode materials. Therein, the existence of porous structure can effectively promote the contact between electrode materials and electrolyte, and buffer the volume change during cycling. Besides, an effective carbon coating or combining with porous cobalt based oxides can further improve the electrochemical performances based on elevated electron conductivity [4-20].

Aroused by these, an initial synthesis of porous cobalt based oxides, and subsequent surface coating or composite with carbon materials has been greatly developed for their use as LIBs anodes. Taking CoO as examples, the N doped carbon coated hollow CoO nanocubes prepared from *in situ* carbonization/reduction of Co_3O_4 nanocubes/polypyrrole composite can reveal a discharge capacity of 598.3 mAh g^{-1} after 50 cycles, which is much better than the precursor Co_3O_4 [22]. The CoO hollow cube/reduced graphene oxide composite can provide a discharge capacity of 1170 mAh g^{-1} at the current density of 150 mA g^{-1}, and 94% of this value can be retained at the 60th cycle. In contrast, the bare CoO only delivers a reversible capacity value less than 900 mAh g^{-1}, and 60% of the total value will be lost at same condition [23]. In present study, the CoO nanorods @ N-doped carbon has been prepared using porous Co_3O_4 nanorods as template, and the polypyrrole formed on the surface of Co_3O_4 nanorods are used as reduction and carbon source [22, 24-28]. The influences of various pyrrole contents (polypyrrole monomer) on the structures and electrochemical performances of target products have been also clearly studied in the text.

2. EXPERIMENTAL

2.1 Synthesis of porous Co_3O_4 nanorods

All of reagents were analytical grade and used as received. The porous Co_3O_4 nanorods were prepared by an oxalate precipitation and subsequent calcination route: 50 mL of $CoCl_2$ solution (0.1 mol/L) was slowly added into 50 mL of oxalate solution (0.2 mol/L) under stirring at a temperature of 60^oC. Then, the mixed solution was kept at 60^oC for 2 h, and the pink precipitation was filtered and washed with water and ethanol. After drying, the pink powder was annealed at 300^oC for 4h under air condition to obtain the black Co_3O_4.

2.2 Synthesis of porous CoO nanorods @ N-doped carbon

0.25 g of as-prepared porous Co_3O_4 nanorods was added into 100 mL of sodium dodecyl benzene sulfonate (SDBS; 2 g) solution under vigorous stirring. The mixed solution was initially treated by ultrasonication for ~15 min, and then a certain amount of pyrrole monomer was added into above suspension under stirring. After that, the solution was kept at room temperature for 0.5 h, and 10 mL of $Na_2S_2O_8$ solution (0.1 mol/L) was added as initiator. The polymerization process was maintained for about 12 h to obtain Co_3O_4 nanorods @ poly pyrrole (PPy). Finally, the resultant suspension was centrifuged, washed with water and ethanol several times and dried at 80°C [24]. After treatment at 450°C for 4 h under Ar atomsphere, the Co_3O_4 nanorods @ PPy can be converted into CoO @ N-doped carbon.

2.3 Structural characterization

The crystal phases were recorded on a powder X-ray diffractormeter (DX-2700, Dandong) with Cu-Kα radiation (40 kV, 30 mA) and 0.06 degree/s in the 2θ range of 10 and 80°. The morphologies, surface structures and energy dispersive X-ray spectrometer (EDS) mapping were observed using JEOL JSM-7500F scanning electron microscope (SEM, 5 kV), and transmission electron microscopy (TEM), High-resolution TEM (HRTEM) and selected area electron diffraction (SAED) measurement were performed on JEM-2100F transmission electron microscope (TEM, 100 kV).

2.4 Electrochemical measurement

All the electrochemical measurements were carried out using CoO @ N-doped carbon/Li coin cells (CR 2016) at room temperature. Active materials (i.e., as-prepared materials), binder sodium alginate and conductive agent acetylene carbon were well ground in an agate mortar at a weight ratio of 7:2:1. The resulting mixtures were slurried by deionized water, pasted onto copper foils, dried at 80°C for about 5 h under air, and then cut into discs with a diameter of 14 mm. polymer (celgard 2400) and commercial LBC 301 LiPF$_6$ solution (Shenzhen CAPCHEM) were used as separator and electrolyte, respectively, and the coin cells were assembled in an argon-filled glove box. Galvanostatic cycling tests were carried out on a Neware CT-3008 battery test system within a voltage region of 0.01-3.0 V (vs. Li$^+$/Li) at current densities within 200-1000 mA g^{-1}. Cyclic Voltammetry (CV) studies were conducted on a CHI660C Electrochemical Workstation (Shanghai Chenhua) at a scanning rate of 0.1 mV s^{-1} between 0.01 and 3.0 V.

3. RESULTS AND DISCUSSION

The schematic formation process of CoO nanorods @ N-doped carbon from Co_3O_4 nanorods precursor is shown in Fig. 1. Initially, the Co_3O_4 nanorods can be well dispersed under stirring in the

presence of surfactant (i.e., SDBS) [22, 24-28]. Thus, the surface of nanorods can provide nucleation sites for polymerization of pyrrole, and the intermediate Co_3O_4 nanorod/polypyrrole core-shell structure can be obtained.
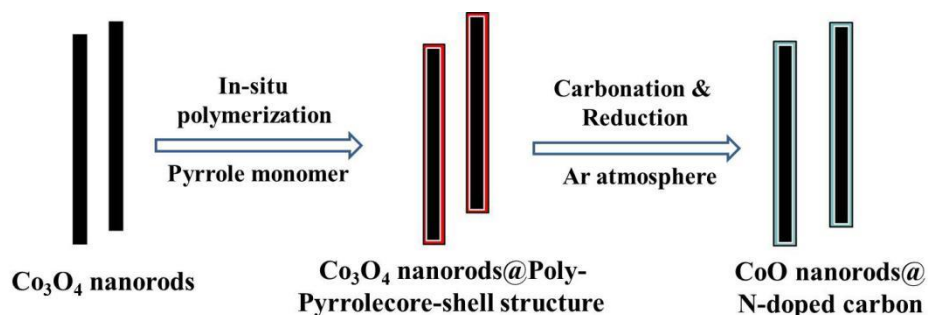

Figure 1. Schematic formation process of CoO nanorods@N-doped carbon from Co_3O_4 nanorods precursor.

After high-temperature calcination under an Ar atomsphere, the Co_3O_4 will be simultaneously reduced to CoO, and a useful carbon layer can be also readily made by the carbonization of residual polypyrrole. Interestingly, the existence of nitrogen element in polypyrrole chain will effectively introduce the nitrogen element into the carbon backbone, resulting in the formation of N doped carbon [22, 24].
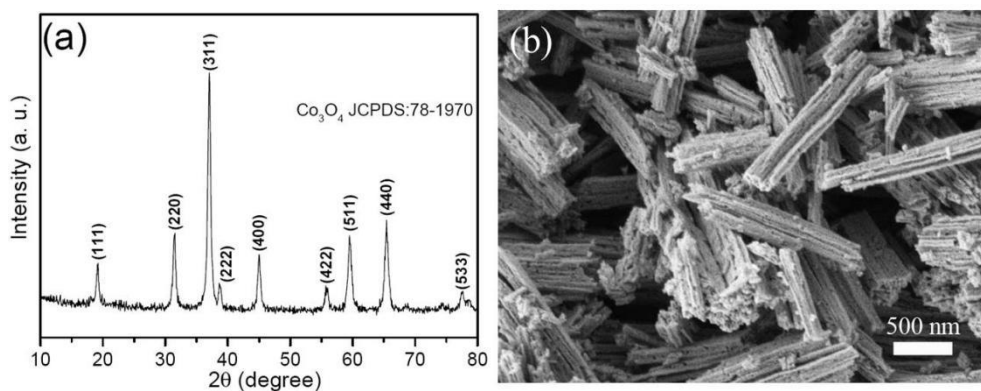

Figure 2. (a) XRD pattern and (b) SEM image of porous Co_3O_4 nanorods.

Fig. 2 shows the XRD pattern and SEM image of precursor porous Co_3O_4 nanorods. All the diffraction peaks of Co_3O_4 in Fig. 2a can be indexed to standard cubic-phase Co_3O_4 (JCPDS: 78-1970), indicating the successful formation of Co_3O_4 from cobalt oxalate. Moreover, the sharp XRD peaks suggest the well construction of cubic Co_3O_4. Fig. 2b exhibits a rodlike structure of precursor Co_3O_4 with the average length within 500 nm-10 μm and the average width of about several hundred nanometers. Some obvious porous structure can be observed on the surface of Co_3O_4 nanorods, which should be attributed to the decomposition of cobalt oxalate.

Using as-prepared porous Co_3O_4 nanorods as template, series products have been prepared by designed experimental route (Fig. 1) in the presence of various pyrrole (polypyrrole monor) contents. Fig. 3 shows the XRD patterns of these products at different amounts of pyrrole. In a low content of pyrrole (i.e., 90 □L), a mixture of Co_3O_4 and CoO can be obtained, indicating the pyrrole with this amount is difficult to be completely reduced into Co_3O_4. When the pyrrole increases to 150 μL, the diffraction peak of Co_3O_4 has been obviously decreased. At a pyrrole content of 180 μL, the diffraction peaks of Co_3O_4 has disappeared, and all diffraction peaks can be ascribed to pure phase CoO (JCPDS: 48-1719), which suggest the samples will possess the structure of CoO once the content of pyrrole exceeds 180 μL [23, 24]. Interestingly, without any other diffraction peaks including metallic Co can be observed from the patterns, meaning the CoO is difficult to be further reduced to metallic Co under present condition.
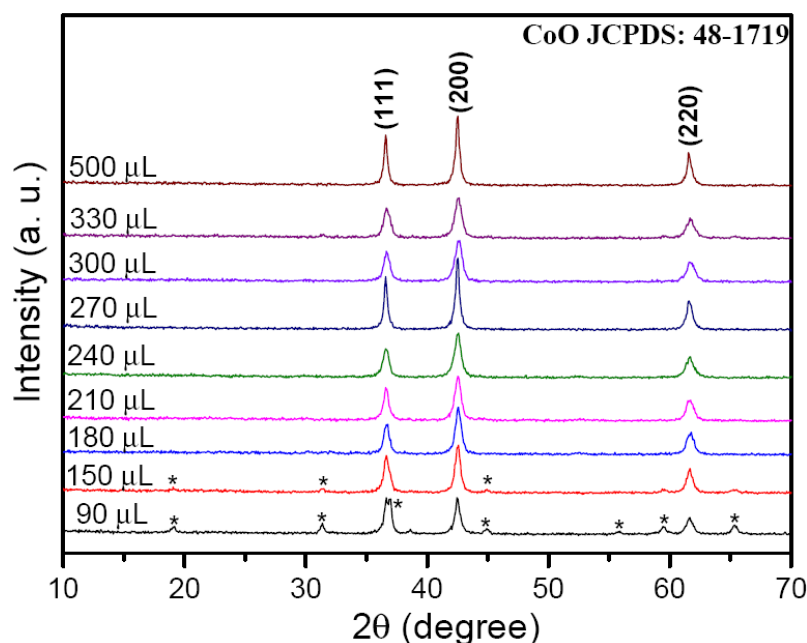

Figure 3. XRD patterns of porous CoO nanorods @ N-doped carbon obtained at different amounts of pyrrole.

At a pyrrole content of 270 μL, the pure phase CoO can be readily made. Therefore, the structure, morphologies and chemical composition of this CoO/carbon composite are studied by SEM, TEM and EDS Mapping. Fig. 4 shows the SEM image of CoO nanorods @ N-doped carbon at the addition of 270 μL pyrrole. The resulting product can well inherit the rodlike structure and porous nature of precursor porous Co_3O_4 nanorods. Especially, these nanorods are endowed with more obvious porous structures (Fig. 4a) due to an additional high temperature reduction. In a magnification image (Fig 4b), it can be seen that the porous nanorods are composed of numerous nanoparticles, and some porous structure can be found among these nanoparticles.
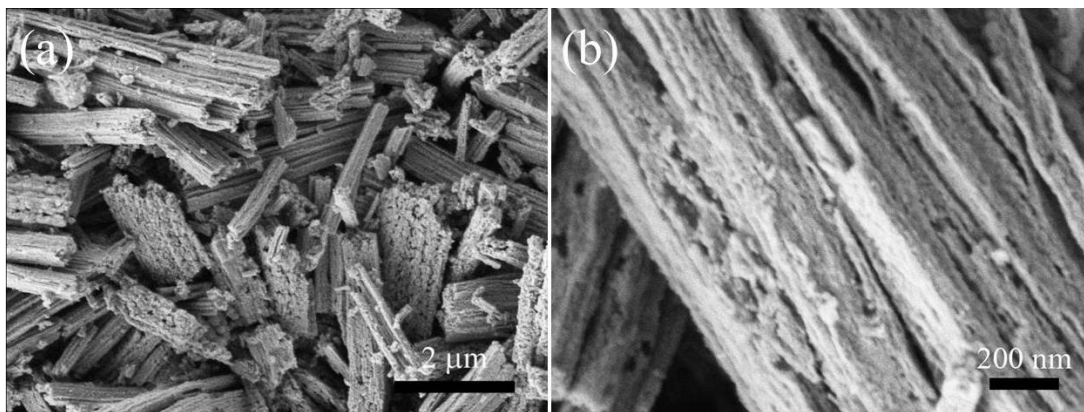
Figure 4. SEM images of porous CoO nanorods @ N-doped carbon with the addition of 270 μL pyrrole.
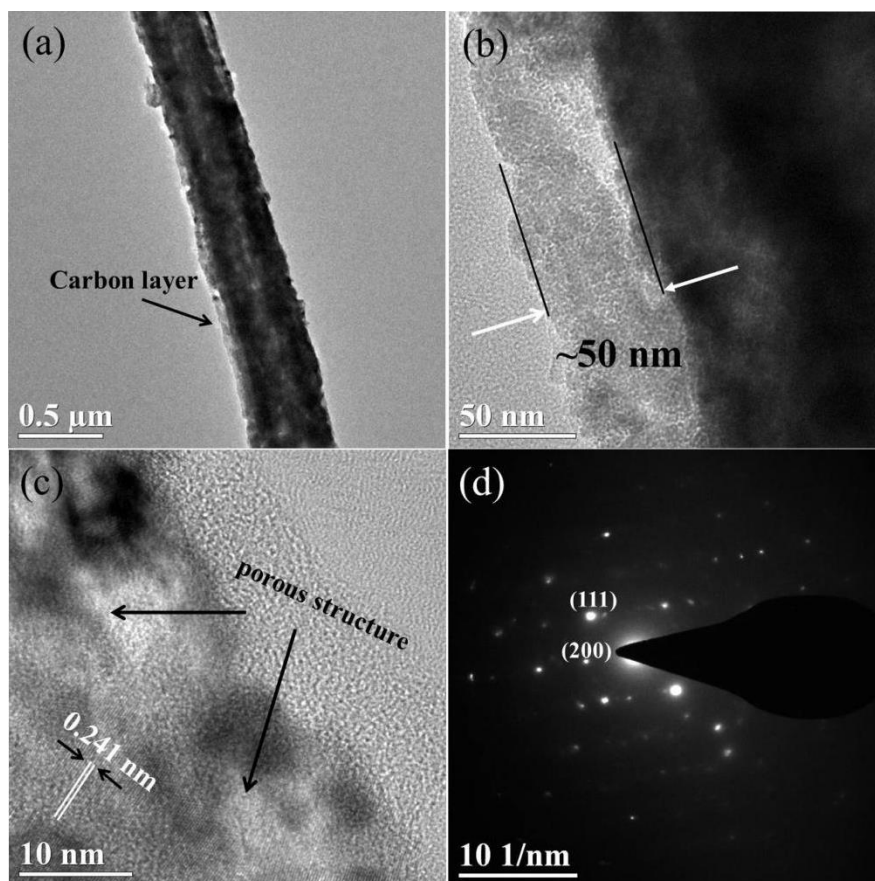

Figure 5. (a) TEM, (b, c) HR-TEM images and (d) SAED pattern of porous CoO nanorods @ N-doped carbon at the addition of 270 μL pyrrole

TEM and HR-TEM measurement have been carried out for further investigating the CoO nanorods @ N-doped carbon composite, as shown in Fig. 5a, b and c. A typical long nanorod with a thin carbon layer structure on the margin can be seen in Fig. 5a, indicating the successful formation of CoO nanorods @ N-doped carbon. In a selected area (Fig. 5b), the thickness of carbon layer can come

to ~50 nm, which is close to the reported literature. In a HRTEM image (Fig. 5c), some porous structure which inherits from porous Co_3O_4 nanorod precursor has been indicated by arrow. Therefore, the as-prepared sample can be defined as CoO nanorods @ carbon. The lattice fringes with a spacing of 0.241 nm can be assigned to the (111) crystal face of cubic CoO (JCPDS: 48-1719). Moreover, the SAED pattern (Fig. 5d) shows the poly-crystalline nature of several nanoparticles, and the diffraction dot such as (111) or (200) crystal face can be detected, which is consistent with the XRD pattern in Fig. 3.
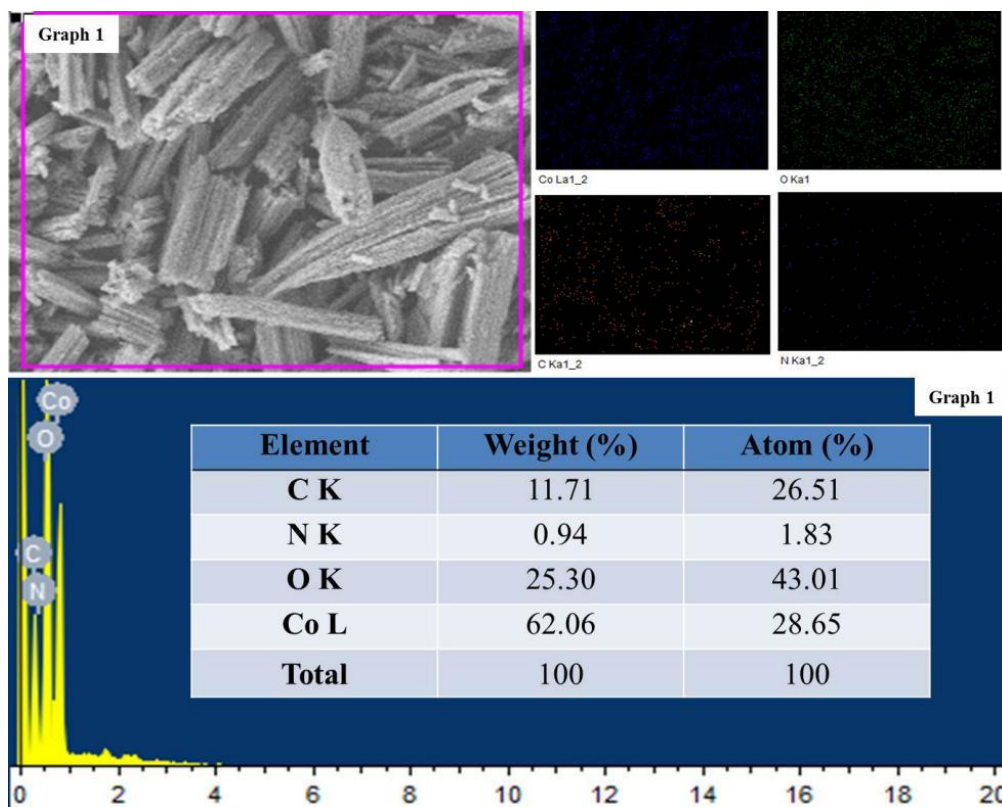

Element	Weight (%)	Atom (%)
C K	11.71	26.51
N K	0.94	1.83
O K	25.30	43.01
Co L	62.06	28.65
Total	100	100

Figure 6. Co, O, C, N element mapping images and EDS analysis in selected area.

Element mapping pattern (Fig. 6) shows the uniformly distribution of Co, O or C element. Some light spot of N element also can be detected from the pattern, proving the co-existence of N element in carbon matrix, which originated from the decomposition of N-contained PPy. From the element analysis, the approximate amount of N element in total carbon is about 6.46%, close to the similar carbon from carbonization of PPy [23, 24]. In fact, the N elements in carbon can effectively improve its electrochemical conductivity, reaction activity, especially hydrophilicity, which is helpful for the preparation of electrode using water soluble binder. The TG curve of CoO nanorods @ N-doped carbon from room temperature to 700°C is revealed in Fig. S1, the estimated weight ratio of carbon should be ~6.7% or more.
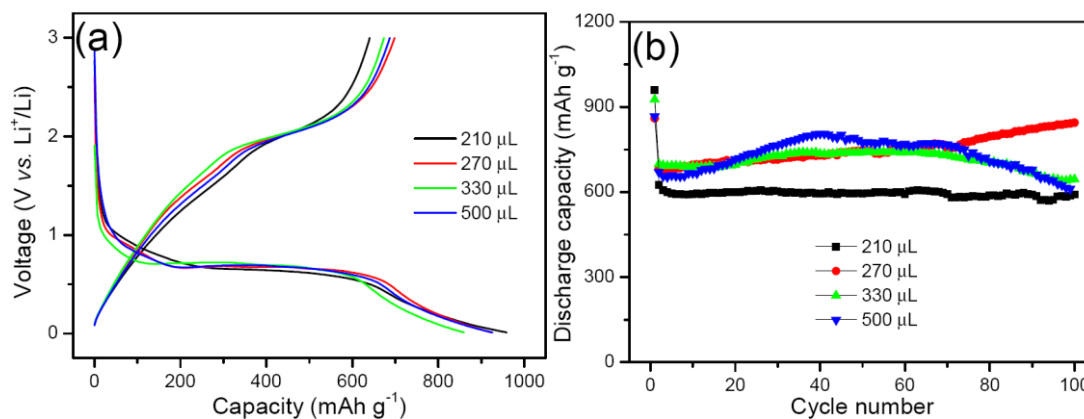
Figure 7. (a) Initial charge-discharge curves and (b) cycling stability of porous CoO nanorods @ N-doped carbon obtained at different amounts of pyrrole.

As lithium ion battery anode, the porous CoO nanorods @ N doped carbon should be suitable. Firstly, the good crystalline, rod-like structure and porous nature of CoO matrix can increase the mechanical stress and buffer the volume change during cycling, thus to improve the cycling stability. Secondly, the existence of surface carbon can effectively improve its electrochemical conductivity, resulting in enhanced rate capability. Fig. 7 shows initial discharge charge and cycling stability curves of CoO nanorods @ N doped carbon composite obtained with different pyrrole contents. When the pyrrole content is 210, 270, 330 or 500 μL, the composite delivers an initial discharge capacity of 959.5, 923.9, 860.1 and 926.3 mAh g^{-1} with a coulombic efficiency of 66.7%, 75.6%, 78.3% or 74.2%, respectively. It can be found that the various pyrrole contents have a great effect on the initial electrochemical behavior of composites, and the sample obtained at the content of 270 and 330 $\square$L have relatively better Coulombic efficiency. As the conversion type LIBs anode material, this Coulombic date (i.e., more than 75%) is not bad, and can be comparative with other literatures [12, 16, 23].

Cycling stability is another important parameter to balance the electrode materials. It can be seen in Fig. 7b, the CoO nanorods @ N doped carbon composite shows a 2nd discharge capacity of 624.8, 679.6, 698.7 or 670.0 mAh g^{-1} at the pyrrole content of 210, 270, 330 or 500 μL. After 100 cycles at 200 mA g^{-1}, a discharge capacity of 586.3, 841.6, 643.5 or 611.1 mAh g^{-1} can be retained, respectively, correspondingly giving capacity retention of 93.8%, 123.8%, 92.1% and 91.2%, respectively. In comparison, the sample from 270 μL has an optimal cycling stability and highest residual discharge capacity at 100th cycle. Interestingly, the capacity evolution during cycling is distinct with each other. In detail, the sample obtained from 210 $\square$L can keep stable discharge capacity after experiencing initial capacity decay. The 270 μL sample still has an increasing tendency even until 100 cycles. The sample from 330 or 500 μL has an increase on the initial 40~50 cycles, and then the capacity decay happen at subsequent cycles. It is a normal phenomenon that the capacity decreases upon cycles. However, the increased discharge capacity upon cycling can be attributed to enhanced interfacial lithium storage for transition metal oxides according to previous reports [29, 30]. The typical charge-discharge curves of 270 μL sample are revealed in Fig. S2. It can be seen that the charge

or discharge curve in 100th cycle is more flat compared with other curve, which is a fact that the sample has undergone interfacial lithium storage.
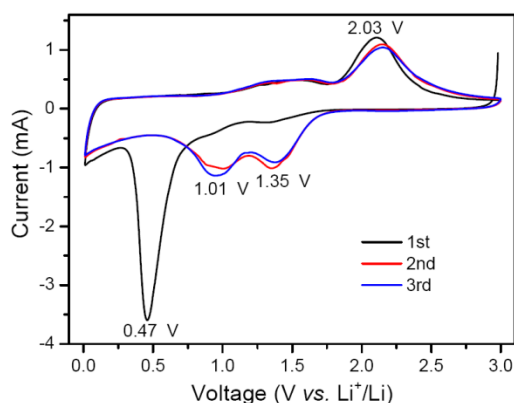

Figure 8. Initial three times CV curve of porous CoO nanorods at the pyrrole content of 270 μL recorded at scanning rate of 0.1 mV S^{-1} within 0.01-3.0 V.

The electrochemical process of as-prepared CoO nanorods @ N-doped carbon is studied by Cyclic Voltammetry test at scanning rate of 0.1 mV s^{-1} between 0.01 and 3.0 V. Fig. 8 reveals an initial cathodic peak nearby 0.47 V can be attributed to the reduction of CoO to metallic Co, as well as the formation of solid-electrolyte interface (SEI) layer. For the subsequent anodic process, a sharp peak of 2.03 V is the reversible oxidation of metallic Co to CoO. At 2nd cycle or later, the cathodic peak shifts to higher voltage and splits into two adjacent peaks (i.e., 1.01 and 1.35 V) because of the decreased surface energy of CoO anode after initial lithiation/delithiation process according to previous literatures [12-14, 22,23].
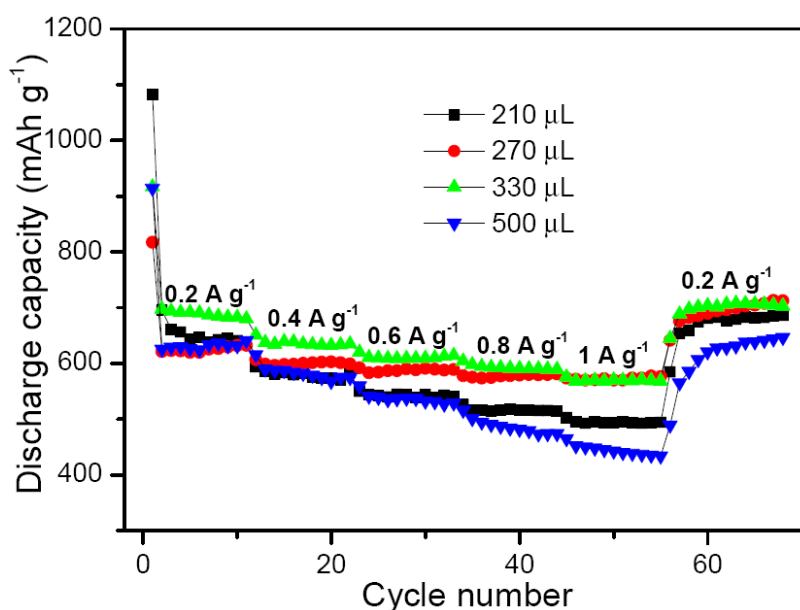

Figure 9. Rate capability of porous CoO nanorods @ N-doped carbon obtained at different amounts of pyrrole.

Table 1. a comparative study of structures and electrochemical performances of various CoO/carbon composite.

Morphology	Preparation route	1st discharge capacity (mAh g^{-1})	Capacity retention	Rate capability (mAh g^{-1})
Intra-stacked CoO/carbon [31]	Wet chemistry	983 (0.1 A g^{-1})	No decay	770 (2 A g^{-1})
CoO@RGO [23]	sacrificial-template	1170 (0.15 A g^{-1})	94% (60 cycles)	654 (0.75 A g^{1})
CoO/C nanofiber [32]	electrospinning	942 (0.1 A g^{-1})	94.9% (65 cycles)	442 (6C)
CoO/carbon [33]	Molten salt route	829.9 (0.07 A g^{-1})	77.3% (50 cycles)	No data
CoO@C nanoarchite-ctures [16]	MOF based material	990 (0.14 A g^{-1})	~95% (30 cycles)	483 (3C)
CoO nanorod/carbon (This work)	carbonization	923.9 (0.2 A g^{-1})	91.1% (100 cycles)	570 (1 A g^{-1})

Rate capabilities of different CoO @ N-doped carbon are revealed in Fig. 9. Each sample experiences a decrease on the discharge capacity upon cycles, and this decrease is not obvious for the 270 and 330 □L sample. For example, the 270 μL sample has a discharge capacity of 622.7 mAh g^{-1} at current density of 200 mA g^{-1}, and the capacity value decreases to 598.3 mAh g^{-1} at 400 mA g^{-1}. Even at a high rate of 1C (1 A g-1), the electrode still keep a discharge value of 570 mAh g^{-1}. Importantly, when the current density goes back to 200 mA g^{-1}, the discharge capacity of this electrode can recover to ~700 mAh g^{-1}. These results indicate the CoO @ N-doped carbon should be promising for high-rate electrochemical process. Especially, a comparative study of structures and electrochemical performances of various CoO/carbon composite is revealed in Tab.1, and it can be found the electrochemical performance of this CoO @ N-doped carbon is not bad.

4. CONCLUSION

Prous CoO nanorods @ N-doped carbon nanocomposites have been prepared by a Co_3O_4 template directed route in the assistance of PPy. The influences of pyrrole contents have been clearly studied, and the pure-phase CoO can be obtained when its content exceed 150 μL. At a pyrrole content of 270 μL, the obtained CoO with surface carbon coating presents obvious porous structure. As LIBs anode, this sample deliver a discharge capacity of 841.6 mAh g^{-1} at 200 mA g^{-1} even after 100 cycles, and a discharge capacity of 570 mAh g^{-1} can be kept at a high rate of 1000 mA g^{-1}. Anyway, the improved electrochemical performance should be beneficial from porous structure and surface carbon coating.

References

1. P. Poizot, S. Laruelle, S. Grugeon, L. Dupont, J.M. Tarascon, *Nature*, 407 (2000) 496-499.

2. Z.Y. Wang, L. Zhou, X.W. Lou, *Adv. Mater.*, 24 (2012) 1903-1911.
3. C.Z, Yuan, H.B. Wu, Y. Xie, X.W. Lou, *Angew. Chem. Int. Ed.*, 52 (2013) 2-19.
4. J.Y. Wang, N.L. Yang, H.J. Tang, Z.H. Dong, D. Kisailus, Z.Y. Tang, D. Wang, *Angew. Chem. Int. Ed.*, 52 (2013) 6417-6420.
5. N. Yan, L. Hu, Y. Wang, H. Zhong, X.Y. Hu, X.K. Kong, Q.W. Chen, *J. Phys. Chem. C*, 116 (2012) 7227-7235.
6. Y.H. Dou, J.T. Xu, B.Y. Ruan, Z.Q. Sun, S.X. Dou, *Adv. Energy Mater.*, 8 (2016) DOI: 10.1002/aenm.201501835.
7. G.L. Xu, J.T. Li, L. Huang, W.F. Lin, S.G. Sun, *Nano Energy*, 3 (2013) 394-402.
8. H.H. Li, Z.Y. Li, X.L. Wu, L.L. Zhang, H.F. Wang, H.Z. Sun J.P. Zhang, *J. Mater. Chem. A*, 4 (2016) 8242-8248.
9. C.X. Peng, B.D. Chen, Y. Qin, S.H. Yang, C.Z. Li, S.Y. Liu, J.H. Yang, *ACS Nano*, 2 (2012) 1074-1081.
10. Y.M. Sun, X.L. Hu, W. Luo, Y.H. Huang, *J. Phys Chem. C*, 116 (2012) 20794-20799.
11. J. Jiang, J.P. Liu, R.M. Ding, X.X. Ji, X.T. Huang, *J. Phys Chem. C*, 114 (2010) 929-932.
12. H. Guan, X. Wang, H.Q. Li, C.Y. Zhi, T.Y. Zhai, D. Golberg, *Chem. Commun.*, 48 (2012) 4878-4880.
13. Y.M. Sun, X.L. Hu, W. Luo, Y.H. Huang, *J. Mater. Chem.*, 22 (2012) 13826-13831.
14. Y. Qi, H. Zhang, N. Du, D.R. Yang, *J. Mater. Chem. A*, 1 (2013) 2337-2342.
15. M. Zhang, F.L. Yan, X. Tang, Q.H. Li, G.Z. Cao, *J. Mater. Chem. A*, 2 (2014) 5890-5897.
16. J. Liu, Y.C. Zhou, C.P. Liu, J.B. Wang, Y. Pan, D.F. Xue, *CrystEngComm*, 14 (2012) 2669-2674.
17. Y.J. Wang, J. Ke, Y.W. Zhang, Y.H. Wang, *J. Mater. Chem. A*, 3 (2015) 24303-24308.
18. J.X. Fu, W.T. Wong, W.R. Liu, *RSC Adv.*, 5 (2015) 75838-75845.
19. W. Luo, X.L. Hu, Y. Sun, Y.H. Huang, *J. Mater. Chem.*, 22 (2012) 8916-8921.
20. 20 J. Bai, X.G. Li, G.Z. Liu, Y.T. Qian, S.L. Xiong, *Adv. Funct. Mater.*, 24 (2014) 3012-3020.
21. Y.W. Zhang, X.Y. Wang, Q.L. Zhao, Y.Q. Fu, H.B. Shu, *Electrochim. Acta*, 180 (2015) 866-872.
22. K.W. Xie, P. Wu, Y.Y. Zhou, Y.M. Zhou, T.H. Lu, *ACS Appl. Mater. Interfaces*, 6 (2014) 10602-10607.
23. X. Guan, J.W. Nai, Y.P. Zhang, P.X. Wang, L. Guo, *Chem. Mater.*, 26 (2014) 5958-5964.
24. X. Gu, J. Yue, L. Chen, S. Liu, J. Yang, Y.T. Qian, X.B. Zhao, *J. Mater. Chem. A*, 3 (2015) 1037-1041.
25. Z.G. Yin, Y.H. Ding, Q.D. Zheng, L.H. Guan, *Electrochem. Commun.*, 20 (2012) 40-43.
26. L. Zhan, H.B. Chen, J.Q. Fang, S.Q. Wang, H.H. Zhang, *Electrochim. Acta*, 209 (2016) 192-200.
27. J.J. Yuan, C.H. Chen, Y. Hao, C.L. Wang, Y.M. Xie, *J. Alloys Compd.*, 691 (2017) 34-39.
28. M. M. Ren, F.Y. Li, W.L. Liu, L. W. Su, *ChemElectroChem*, 4 (2017) 2862-2869.
29. S.Q. Zhao, F. Feng, F.Q. Yu, Q. Shen, *J. Mater. Chem. A*, 3 (2015) 24095-24102.
30. F. Feng, S.Q. Zhao, R. Liu, Z.W. Yang, Q. Shen, *Electrochim. Acta*, 222 (2016) 1160-1168.
31. C.J. Chae, K.W. Kim, S.S. Lee, S. Choi, *Nanoscale*, 7 (2015) 10368-10376.
32. M. Zhang, E. Uchaker, S. Hu, G.Z. Cao, *Nanoscale*, 5 (2015) 12342-12347.
33. S.S. Chu, C. Yang, X. Xia, X.T. Su, *New J. Chem.*, 40 (2016) 2722-2729.